AIAA JOURNAL
Vol. 48, No. 3, March 2010

# Damage Detection in a Plate Using Beam-Focused Shear-Horizontal Wave Magnetostrictive Patch Transducers

Ju Seung Lee* and Hoe Woong Kim†
*Seoul National University, Seoul 151-742, Republic of Korea*
Byung Chul Jeon‡
*Aero Technology Research Institute, Daegu 304-160, Republic of Korea*
Seung Hyun Cho§
*Korea Research Institute of Standards and Science, Daejon 305-340, Republic of Korea*
and
Yoon Young Kim¶
*Seoul National University, Seoul 151-742, Republic of Korea*

DOI: 10.2514/1.44895

**For efficient nondestructive ultrasonic inspection in plate/shell structures, the development of a guided-wave based method using transducers having good beam directivity, high power, and little dispersion is important. To this end, a damage inspection strategy using a set of specially designed magnetostrictive patch transducers capable of generating beam-focused, nondispersive shear-horizontal waves is proposed. In the present ultrasonic pitch–catch inspection, only a few single transducers need to be installed around an inspection area. To convert measured wave signals by the transducers into two-dimensional images, a relatively simple yet effective data-processing technique suitable for the employed transducer setting is developed. Sets of experiments were conducted on rectangular plates having one or two circular holes with a diameter of 1 or 3 millimeters. For all experiments, the Gabor-shaped ultrasonic pulses having the center frequencies of 250 kHz and 360 kHz were used.**

## Nomenclature

| | | |
|---|---|---|
| $A^n$ | = | region of influence for a grid point $n$ |
| $c_s$ | = | shear wave speed |
| $D$ | = | interval between solenoids in planar solenoid array |
| $E^n_{i,j}(t)$ | = | envelope of the voltage output signal at a specific arrival time $t$ from $i$ to $j$ via $n$ |
| $f$ | = | center frequency |
| $G$ | = | spacing between virtual grid points |
| $h_n$ | = | the size of $A^n$ |
| $I_{i,j}(p)$ | = | squared magnitude of the wave scattered from an arbitrary point $p$ when $(T_i, R_j)$ is used |
| $I^n_{i,j}(n)$ | = | squared magnitude of the wave scattered from a grid point $n$ when $(T_i, R_j)$ is used |
| $I(p)$ | = | intensity used to image the inspected area $S$ |
| $l_{i\text{-}n}$ | = | distance between $i$ and $n$ |
| $l_{i\text{-}p}$ | = | distance between $i$ and $p$ |
| $l_{n\text{-}j}$ | = | distance between $n$ and $j$ |
| $l_{p\text{-}j}$ | = | distance between $p$ and $j$ |
| $M$ | = | total number of the used transducers |
| $N$ | = | total number of grid points |
| $n$ | = | virtual grid point number of location |
| $R_j$ | = | planar solenoid array-type orientation-adjustable patch-type magnetostrictive transducer working as a receiver at location $j$ |
| $S$ | = | inspection region |
| $T_i$ | = | planar solenoid array-type orientation-adjustable patch-type magnetostrictive transducer working as a transmitter at location $i$ |
| $t$ | = | time or an arrival time |
| $t_{i\text{-}n}$ | = | traveling time from $i$ to $n$ |
| $t_{i\text{-}n\text{-}j}$ | = | total time of flight from $i$ to $j$ via $n$ |
| $t_{i\text{-}p}$ | = | traveling time from $i$ to $p$ |
| $t_{i\text{-}p\text{-}j}$ | = | total time of flight from $i$ to $j$ via $p$ |
| $t_{n\text{-}j}$ | = | traveling time from $n$ to $j$ |
| $t_{p\text{-}j}$ | = | traveling time from $p$ to $j$ |
| $V^n_{i,j}(t)$ | = | voltage signal of measured waves at a specific arrival time $t$ from $i$ to $j$ via $n$ |
| $x_n, y_n$ | = | Cartesian coordinate of the grid point $n$ |
| $x_p, y_p$ | = | Cartesian coordinates of an arbitrary point $p$ |
| $\sigma$ | = | parameter controlling the effective time width of the Gabor pulse |
| $\phi$ | = | phase of the Gabor pulse |

*Subscripts*

| | | |
|---|---|---|
| $i$ | = | index denoting transmitter location |
| $j$ | = | index denoting receiver location |
| $p$ | = | arbitrary location (or point) inside $S$ |

Presented as Paper 2381 at the 50th AIAA/ASME/ASCE/AHS/ASC Structures, Structural Dynamics, and Materials Conference, Palm Springs, CA, 4–7 May 2009; received 13 April 2009; revision received 22 Nov. 2009; accepted for publication 23 Nov. 2009. 

*Ph.D. Candidate, School of Mechanical and Aerospace Engineering, Shinlim-Dong, San 56-1, Kwanak-Gu; National Creative Research Initiatives Center for Multiscale Design; lee@idealab.snu.ac.kr.

†Ph.D. Candidate, School of Mechanical and Aerospace Engineering; Shinlim-Dong, San 56-1, Kwanak-Gu; National Creative Research Initiatives Center for Multiscale Design; smaky4u@idealab.snu.ac.kr.

‡Captain, Aero Technology Research Institute, Gumda-Dong, Donggu; puurni@empal.com.

§Senior Research Scientist, Center for Safety Metrology, Division of Industrial Metrology, Doryong-Dong 1, Yuseong-Gu; seungcho@kriss.re.kr.

¶Professor, School of Mechanical and Aerospace Engineering, Shinlim-Dong, San 56-1; Kwanak-Gu; Director, National Creative Research Initiatives Center for Multiscale Design; yykim@snu.ac.kr. Member AIAA.

## I. Introduction

THE main advantage of using guided waves for damage inspection in plate or shell structures (e.g., aircraft fuselage/wing, ship hulls, and oil/gas storage, etc.) is that a large portion of a test structure can be inspected only with a small number of transducer installations. For this reason, numerous investigations using guided waves have been conducted [1–7]. Despite of the effectiveness of guided-wave based damage inspection, more efforts should be made to increase beam power, to improve directivity (or focusing), and to use a nondispersive wave mode. Because the issue of beam power is more related to electronics, this work will be mainly concerned with beam directivity (or focusing) and wave dispersion here. Perhaps the most common beam focusing approach is a phased-array technique. Because this technique requires a large number of piezoelectric transducers or electromagnetic acoustic transducers (EMAT) for good focusing [8–12] it costs much, especially when damage detection is considered in a large structure. In addition, the phased-array method requires sophisticated time delay algorithm for beam focusing.

In this work, an alternative patch-type magnetostrictive transducer recently developed by Lee et al. [13] will be employed. Without forming a phased array, this transducer was shown to effectively focus the generated wave beam along a target direction in a plate. It was also shown that it can generate and receive a nondispersive shear-horizontal wave mode (the fundamental shear-horizontal wave, SH0) effectively. Because the nondispersive guided wave has a constant group velocity for all frequencies, the generated waveform from a transmitter preserves its shape as it propagates. Therefore, the SH0 mode is most preferred for a guided-wave based nondestructive evaluation of a platelike structure. Also, the displacement and the stress of the SH0 mode are uniform through the thickness of a plate so that its sensitivity to a defect does not depend on the through-thickness location of a defect. On the other hand, it is not so easy to generate shear waves having good directivity by using piezoelectric transducers. Therefore, most piezoelectric transducer based inspection techniques tend to employ the dispersive Lamb waves and use some signal processing algorithms to compensate the dispersion effects of the Lamb waves [14–17]. In this work a simple, efficient damage inspection technique, based on a recently developed magnetostrictive transducer, will be presented.

Because the magnetostrictive transducer of Lee et al. [13] has quite different characteristics from those of piezoelectric transducers, a damage detection strategy suitable for the magnetostrictive transducer may be employed. In particular, an efficient 2-D imaging technique using a set of single magnetostrictive transducers will be developed in this investigation. Before presenting the proposed damage inspection method using the magnetostrictive transducer, a brief introduction of the damage inspection setup and the characteristics of the magnetostrictive transducers will be given below.

Figure 1a shows a schematic of magnetostrictive transducer based damage inspection in a plate, while Fig. 1b the configuration of the magnetostrictive transducer of Lee et al. [13], called the Planar Solenoid Array-type Orientation-adjustable Patch-type Magnetostrictive Transducer (PSA-OPMT). The symbols P1 and P2 in the figure denote PSA-OPMTs installed on a test plate. As shown in Fig. 1b, PSA-OPMT consists of a circular magnetostrictive patch bonded on a plate and a specially configured magnetic circuit composed of two permanent magnets and a Planar Solenoid Array (PSA). In generating and measuring elastic waves by the magnetostrictive patch, the magnetostrictive effect, referring to the coupling phenomenon between magnetic field and mechanical stress, [18] is used. The following is a brief summary explaining how shear-horizontal (SH) ultrasonic waves are generated and measured by PSA-OPMTs. See Lee et al. [13] for more detailed accounts of the working principle of PSA-OPMT.

1) Two permanent magnets supply a bias magnetic field in a circular magnetostrictive patch which mainly flows along the *y* direction. The bias field is indicated by dashed arrows in Fig. 1c.

2) When an input current is sent to PSA each solenoid will develop a dynamic magnetic field in the negative and positive directions, as depicted in the zoomed view of PSA shown in Fig. 1b, because of the coil winding pattern, clockwise or counterclockwise. Then, the dynamic magnetic field generated by PSA is applied to the circular

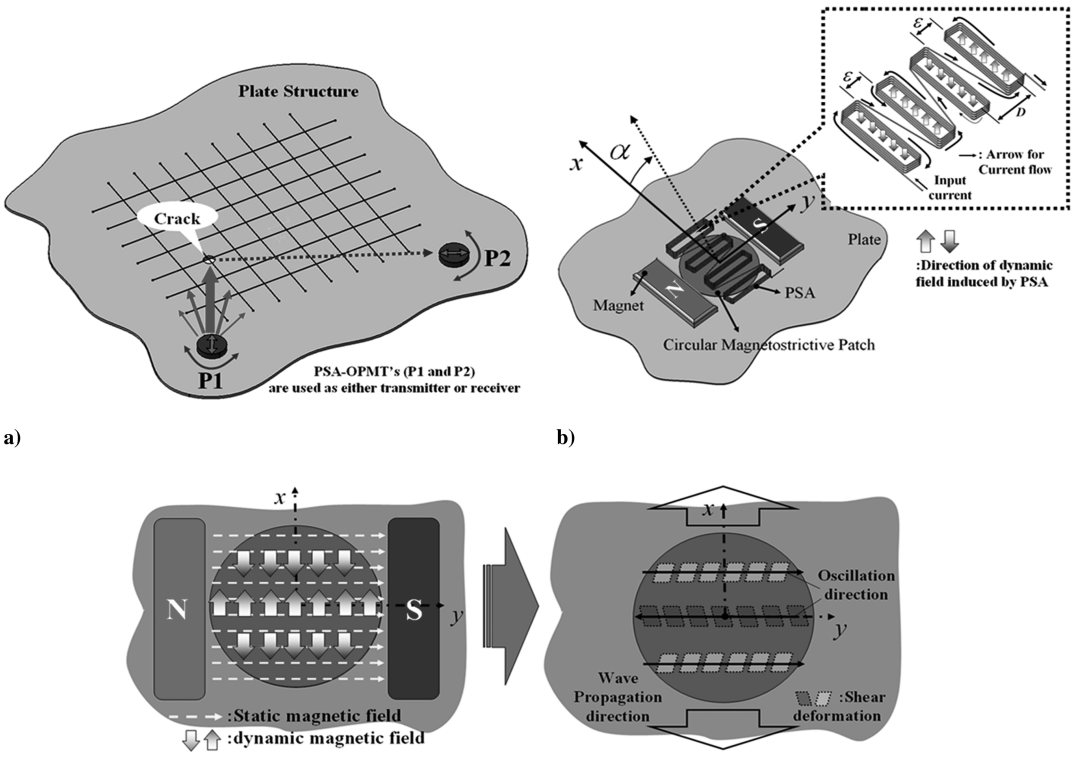


**Fig. 1 a) Schematics of pitch–catch guided-wave damage detection in a plate by using two PSA-OPMTs denoted by P1 and P2 (in this figure P1 and P2 work as a transmitter and a receiver, respectively), b) the configuration of PSA-OPMT, and c) the working principle of PSA-OPMT.**

magnetostrictive patch bonded to a test plate in the positive and negative $x$ directions as depicted in Fig. 1c.

3) Because two magnetic fields are orthogonal to each other, shear strains are developed in the patch as illustrated in Fig. 1c by the Wiedemann effect [19,20], a special case of the magnetostrictive effect.

4) The dynamic strain developed in the patch serves as a time-varying SH wave actuation source of the plate because the patch is bonded to the plate. The SH wave then propagates as a guided wave in the plate.

5) If the distance $D$ in Fig. 1b is so adjusted as to be related to the wavelength of the used ultrasonic wave pulse, the generated wave beam can be highly focused mainly along the $x$ axis as indicated in Fig. 2.

6) In focusing beam along the $x$ axis, the planar solenoid array configuration plays an important role.

Figure 2a shows a pitch–catch experiment setup using two PSA-OPMTs, and Fig. 2b shows the wave radiation pattern of the first nondispersive mode (SH0) of shear waves obtained by experiments and theoretical analysis at two center frequencies, 250 kHz and 360 kHz. For theoretical analysis, a 2-D distributed line source model developed in [13] was employed. The alternating signs of shear strains along source lines were taken into account. Note that good directivity was achieved only with single transducers without forming phased arrays. Figure 2b clearly demonstrates that beam directivity becomes better as the center frequency becomes higher. This is because the beam divergence angle in the far field region is proportional to the wavelength $\lambda$ ($\lambda = c_s/f$) of the generated (received) shear wave.

This paper is organized as follows. The next section is devoted to the development of a damage inspection technique using ultrasonic guided-wave signals obtained by a set of PSA-OPMTs. In particular, a PSA-OPMT based experimental strategy and a 2-D imaging technique by using the acquired signals will be developed. In the subsequent section, the effectiveness of the developed method will be tested experimentally. All experiments were conducted on 0.8 mm thick aluminum plates having one or two holes with a diameter of 1 mm or 3 mm. The effects of the excitation frequencies on the processed images will be also examined. The summary and conclusions of this research will then follow.

## II. Planar Solenoid Array-Type Orientation-Adjustable Patch-Type Magnetostrictive Transducer Based Damage Detection Method

In this section, the proposed damage detection method using PSA-OPMTs will be presented. An imaging algorithm will be given after data acquisition and processing strategies are presented. The underlying wave mechanics related to PSA-OPMTs will be also briefly explained.

### A. Data Acquisition and Preprocessing

Figure 3a schematically shows the experimental setup; only a few PSA-OPMTs are installed on a test plate. An inspection region of a plate is surrounded by PSA-OPMTs. Because PSA-OPMTs have good directivity as demonstrated in Fig. 2, the main wave power can be so adjusted as to target on a specific point, say point 12 in Fig. 3a. This means that if the P1 transducer is used as a transmitter, the main power of the generated wave by P1 is directed at point 12, and if the P2 and P3 transducers are used as receivers, they are also directed at point 12 to detect reflected waves if there is any defect near point 12. The big arrows in Fig. 3a denote the focusing directions of the transducers. Because the assembly of two permanent magnets and a planar solenoid array is separated from the circular patch bonded to a test plate, one can easily adjust the wave propagation direction (the $x$ axis in Fig. 1b) by rotating the assembly. (In fact, the rotation is automated by a step motor as shall be explained in the next section.)

Note that the transmitted and received ultrasonic wave by PSA-OPMTs can be nondispersive as long as the excitation frequency is below the cutoff frequency of the second shear-horizontal wave mode (see Fig. 4 for the dispersion curve of an aluminum plate used for experiments). In this case, the time of flight of the SH0 wave can be easily calculated by using the shear wave speed, $c_s$–this is a critical advantage of using PSA-OPMTs to generate and measure the SH0 mode. In all experiments, waves of the Gabor pulse form will be used:

$$g(t) = e^{-t^2/2\sigma^2}\cos(2\pi f t + \phi)(t\text{: time}, \phi\text{: phase}) \qquad (1)$$

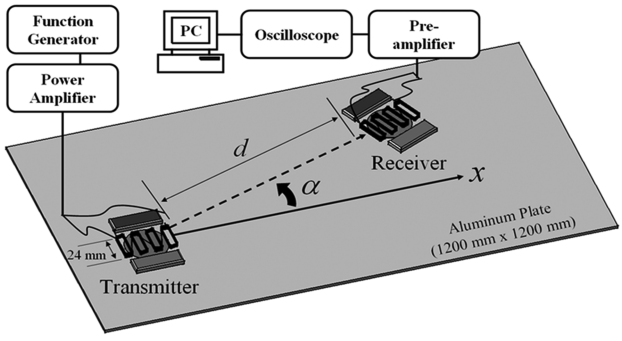


a)

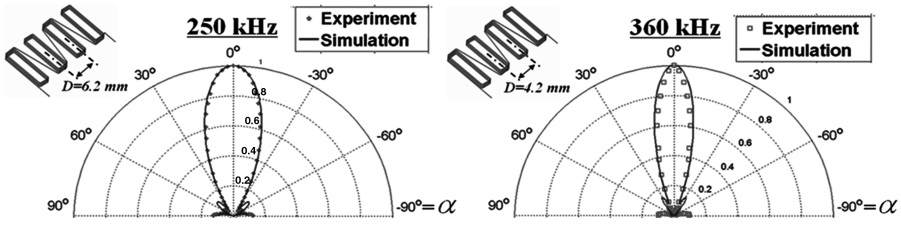


b)

**Fig. 2 a) Pitch–catch experimental setup using two PSA-OPMTs, b) wave radiation patterns of the SH0 wave mode by PSA-OPMTs at the excitation frequencies of 250 kHz ($D = 6.2$ mm) and 360 kHz ($D = 4.2$ mm). (The orientation angle $\alpha$ is defined in Fig. 1.)**

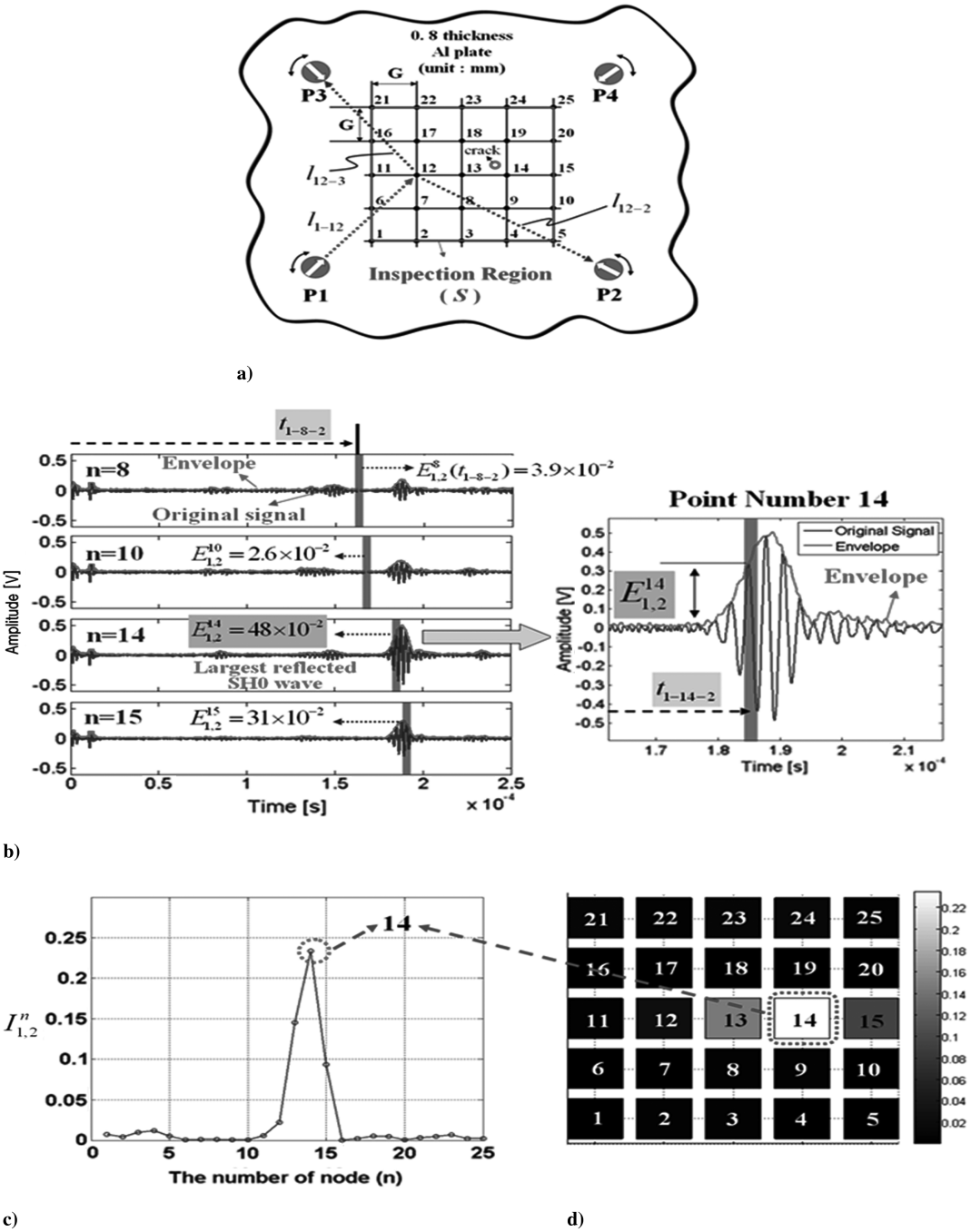


**Fig. 3 a) Schematics of wave data acquisition by using PSA-OPMTs in a 0.8 mm aluminum plate having a 3 mm hole crack, b) measured time signals by P2 for different target grid points (sampling time: 5 x $10^{-8}$ s), c) the squared magnitude $I^{n}_{1,2}$ of the scattered wave from grid point $n$ measured by a transducer P2 for the transmitting transducer P1, and d) an illustrative 2-D image of a plate by elementary data process.**

where $\sigma$ is a parameter controlling the effective time-width of the pulse and $f$, the center frequency. The Gabor wave form is used because it has the best time-frequency resolution [21]. In this study, $\sigma = 4.8 \times 10^{-6}$ sec and $\phi = 0$ rad were used. When a planar solenoid array is used, the distance $D$ is so selected as to generate a Gabor pulse of the center frequency $f$ effectively. The relation between $D$ and $f$ is given by [13]

$$2D \simeq \lambda = \frac{c_s}{f} \tag{2}$$

where $\lambda$ is the wavelength.

Points 1–25 in Fig. 3a denote virtual grid points that will be the targeting points of PSA-OPMTs. For simplicity, the grid distance along the horizontal and vertical axes is assumed to be the same as $G$. In the test problem shown in Fig. 3a, a small crack is located near point 14. The following is the procedure to acquire guided wave data.

1) Identify an inspection region $S$ and locate a few PSA-OPMTs to cover $S$. In the case of Fig. 3a, four PSA-OPMTs (P1, P2, P3, and P4) are installed on a 0.8 mm thick aluminum plate.

2) Virtually discretize the inspection region and get the coordinates of the virtual grid points. For simplicity, a uniform distance of $G$ will be used.

3) Select a transmitting transducer and receiving transducers for pitch–catch experiments. For example, P2 and P3 are used as receivers ($R_j$) while P1 is used a transmitter ($T_i$). Symbols $i$ and $j$ are indices denoting the location of a transmitter ($T$) and the location of receiver ($R$), respectively. It is noted that the additional use of P4 does not give much useful information so only P2 and P3 are used as receivers in this case.

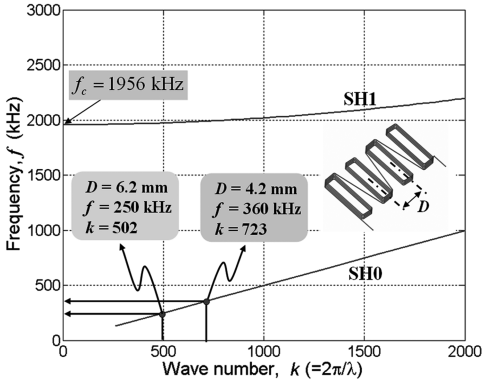


**Fig. 4 The dispersion relation of two SH wave modes for a 0.8 mm thick aluminum plate ($f_c$: the cutoff frequency).**

4) Choose a target point and direct P1, P2, and P3 toward the point. Then supply current of the Gabor pulse form to PSA of the transmitter (P1) and the propagated wave in a plate is measured by PSAs of receivers (P2 and P3) as voltage output. For instance, the received signals by P2 for target points of $n = 8$, 10, 14 and 15 are plotted in Fig. 3b where $n$ indicates the grid point number.

5) Repeat Step 4 to cover all grid points in the inspection region.

6) If necessary, change the role of transmitters and receivers; for instance, choose P2 as a transmitter and (P1, P4) as receivers. Repeat this step if necessary.

To facilitate the time-of-flight calculation, measured signals by receivers are processed by the Hilbert transform [22] and the resulting signal envelopes are denoted by thick lines in Fig. 3b. Thus, the envelope $E^n_{i,j}(t)$ denotes the magnitude of the voltage output $V^n_{i,j}(t)$ sensed at an arrival time $t$ by a receiver $R_j$ for the ultrasonic wave generated by a transmitter $T_i$ targeting on grid point $n$. If there is a crack at or near the target point $n$, a significant amount of scattered waves by the crack will be received by a receiver $R_j$. In that case, the maximum value of $E^n_{i,j}(t)$ will appear at time $t = t_{i\text{-}n\text{-}j}$ where $t_{i\text{-}n\text{-}j}$ is the total time of flight of a wave of a Gabor pulse from $i$ to $j$ via $n$:

$$t_{i\text{-}n\text{-}j} = t_{i\text{-}n} + t_{n\text{-}j} \tag{3}$$

where $t_{i\text{-}n}$ and $t_{n\text{-}j}$ represent the traveling times of the SH0 wave from $i$ to $n$ and from $n$ to $j$, respectively. Because distances $l_{i\text{-}n}$ from $i$ to $n$ and $l_{n\text{-}j}$ from $n$ to $j$ are known and the shear wave speed $c_s$ is available, $t_{i\text{-}n}$ and $t_{n\text{-}j}$ are simply calculated as

$$t_{i\text{-}n} = \frac{l_{i\text{-}n}}{c_s}, \qquad t_{n\text{-}j} = \frac{l_{n\text{-}j}}{c_s} \tag{4}$$

Then, one can estimate the squared magnitude $I^n_{i,j}(n)$ of the wave scattered from grid point $n$ measured by a transducer located at $j$ as

$$I^n_{i,j}(n) = [E^n_{i,j}(t_{i\text{-}n\text{-}j})]^2 \tag{5}$$

The argument $n$ of $I^n_{i,j}(n)$ denotes the wave scattered from grid point $n$. Figure 3c shows the values of $I^n_{1,2}(n)$ for $n = 1$–25 indicated in Fig. 3a. Because a circular crack is located near $n = 14$, the maximum value of $I^n_{1,2}(n)$ is obtained for $n = 14$. Then, one can suspect a presence of a defect near the grid point $n = 14$. One can also image the inspected square area by the value of $I^n_{1,2}(n)$. The resulting gray-level image is illustrated in Fig. 3d. Although resolution in Fig. 3d is too low to be practically used, the procedure explained earlier demonstrates how one can get a 2-D image of the inspected region by using the wave signals from PSA-OPMTs. In the next subsection, a higher-resolution imaging technique particularly suitable for PSA-OPMTs will be developed.

### B. Planar Solenoid Array-Type Orientation-Adjustable Patch-Type Magnetostrictive Transducer Based Imaging Algorithm

To increase image resolution, the easiest way is to increase the number of grid points. We now develop an efficient imaging technique that can considerably increase without increasing the number of grid points. For the time being, the same set of experimental data $E^n_{i,j}(t)$ as used in Sec. II.A is assumed to be used for imaging. For resolution improvement, the following technique is developed.

First we note that although PSA-OPMTs have good directivity, the generated ultrasound wave from a transmitter $T_i$ propagates in a small region near the target point $n$ because the beam width is finite. Therefore, the scattered wave from a crack located in the small region near $n$ can be sensed by a receiver $R_j$. This means that if there is a crack at a point $p$ near $n$, $E^n_{i,j}(t)$ also includes the scattered wave from the point $p$; see the illustration in Fig. 5. For an experimental setting to record $V^n_{i,j}(t)$ in Fig. 5, we introduce the notion of a so-called region of influence surrounding $n$ in which significant ultrasonic power is delivered. It is surrounded by a dotted line in Fig. 5. The following is the definition of the region $A^n$ of influence for a grid point $n$:

$$A^n = \{(x, y) | x_n - h_n \le x < x_n + h_n, y_n - h_n \le y < y_n + h_n\} \tag{6}$$

where $(x_n, y_n)$ denotes the Cartesian coordinates of the grid point $n$ and $h_n$ the size of $A^n$. The numerical value of $h_n$ is determined by the wave beam spread and the location of $n$, but for simplicity, it will be assumed as

$$h_n = G \quad \text{for all } n \tag{7}$$

If there is a crack at point $p \in A^n$ located at $(x_p, y_p)$, the value of $V^n_{i,j}(t)$ measured at $t = t_{i\text{-}p\text{-}j}$ is the scattered wave from $p$ where

$$t_{i\text{-}p\text{-}j} = t_{i\text{-}p} + t_{p\text{-}j} \tag{8}$$

$$t_{i\text{-}p} = \frac{l_{i\text{-}p}}{c_s}, \qquad t_{p\text{-}j} = \frac{l_{p\text{-}j}}{c_s} \tag{9}$$

In Eqs. (8) and (9), $l_{i\text{-}p}$ and $l_{p\text{-}j}$ denote the distance between $i$ and $p$ and the distance between $p$ and $j$. Finally, the magnitude $I^n_{i,j}(p)$ of the received signal at $j$ by wave scattering at $p$ is determined as

$$I^n_{i,j}(p) = [E^n_{i,j}(t_{i\text{-}p\text{-}j})]^2 \quad \text{for } p \in A^n \tag{10}$$

Because a selected point $p$ can lie inside of four regions of influence enclosing it, we propose to calculate the total magnitude $I_{i,j}(p)$ of the wave signal reflected from $p$ as

$$I_{i,j}(p) = \sum_{n=1}^{N} I^n_{i,j}(p) = \sum_{i=1}^{N} [E^n_{i,j}(t_{i\text{-}p\text{-}j})]^2 \quad \text{for all } p \in S \tag{11a}$$

where

$$I^n_{i,j}(p) \equiv 0 \quad \text{if } p \notin A^n \tag{11b}$$

It is often convenient to normalize $I_{i,j}(p)$ with respect to $I_{i,j}|_{\max}$ for a selected $(i, j)$.

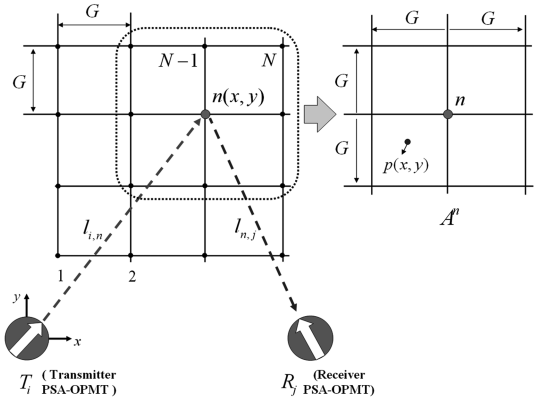


**Fig. 5 The region of influence $A^n$ when a transmitter ($T_i$) and a receiver ($R_j$) target on a grid point $n$.**

Once $I_{i,j}(p)$s are calculated for a specific combination of $(i, j)$, they are calculated for other combinations. If four transducers P1, P2, P3, and P4 are used as illustrated in Fig. 3a, there are four independent combinations of $(i, j)$ such that

$$C = \{(1,2), (1,3), (2,4), (3,4)\} \tag{11}$$

In determining (11) the following reciprocal relation is used

$$I_{i,j}(p) = I_{j,i}(p) \tag{12}$$

When $M$ PSA-OPMTs are installed at different locations, the following intensity measure $I(p)$ is calculated to image the inspected area $S$:

$$I(p) = \prod_{i=1}^{M} \prod_{j=1}^{M} I_{i,j}(p) \quad \text{for all } (i,j) \in C \tag{13}$$

Figure 6 demonstrates the procedure of the proposed imaging technique using PSA-OPMTs. In this example, it is assumed that $N = 9$ and $(i, j) = (1, 2)$ and $(1, 3)$. In comparison with the imaged result in Fig. 3d, the image resolution has been greatly enhanced.

## III. Imaging for Plate Damage Inspection

Using the PSA-OPMT based inspection method presented in the preceding section, a set of shear-horizontal guided-wave experiments were conducted. Four identical PSA-OPMTs covering a square inspection area were used for all experiments. The test plates were 0.8 mm thick aluminum plates. The effectiveness of the proposed PSA-OPMT based inspection method will be investigated and the effects of excitation frequencies and the number of virtual grid points will be also examined.

### A. Experimental Setup

Referring to Fig. 7a and taking the origin of the Cartesian coordinate at P1, the coordinates of P1–P4 are as follows:

$$\text{P1}(0,0), \quad \text{P2}(400,0), \quad \text{P3}(0,400), \quad \text{P4}(400,400) \text{(unit: mm)} \tag{14}$$

The inspection region $S$ is defined as

$$S = \{(x,y) | 100 \le x \le 300, 100 \le y \le 300\} \tag{15}$$

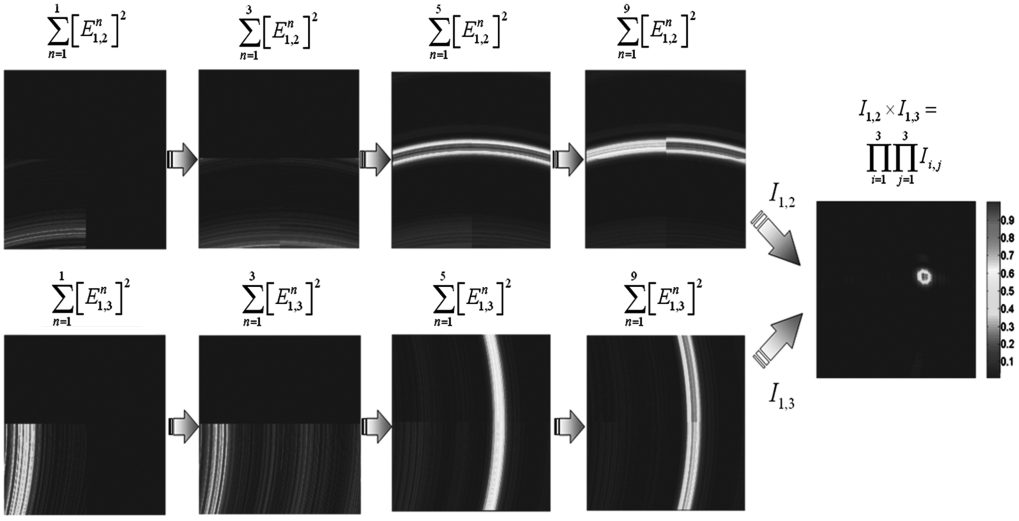


**Fig. 6 Imaging process to explain the concept of the developed imaging method.**

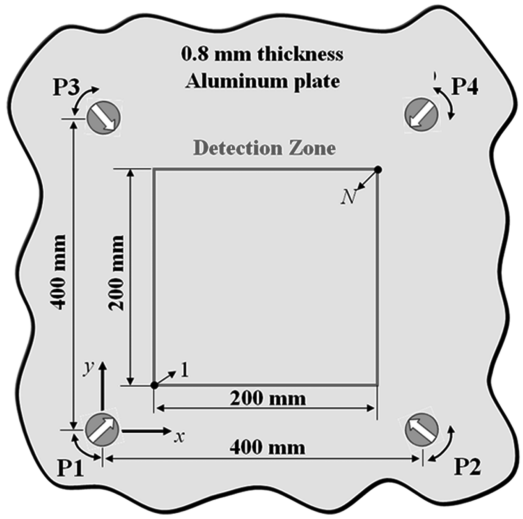


a)

| (unit: mm ) | P1 | P2 | P3 | P4 | 1 | n |
|---|---|---|---|---|---|---|
| x | 0 | 400 | 0 | 400 | 100 | 300 |
| y | 0 | 0 | 400 | 400 | 100 | 300 |

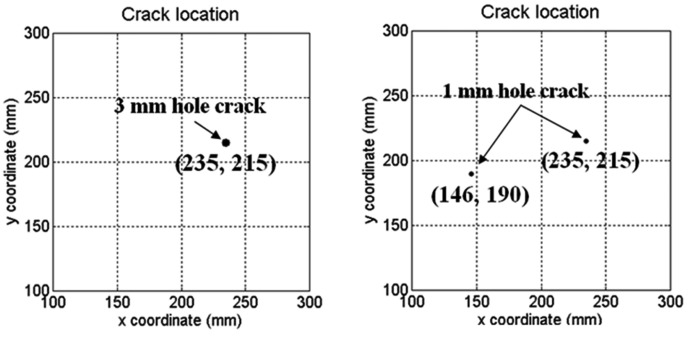


b)

**Fig. 7 a) Schematic view of PSA-OPMT based inspection of an aluminum plate, b) description of two cracked aluminum plates used for the present investigation.**

Two cases of cracked aluminum plates illustrated in Fig. 7b will be inspected:

1) Case 1 consists of a single hole crack $C_1^{(1)}$ having a diameter of 3 mm located at (235, 215).

2) Case 2 consists of two hole cracks $C_1^{(2)}$ at (146, 190) and $C_2^{(2)}$ at (235, 215) having a diameter of 1 mm.

Two excitation frequencies of 250 kHz and 360 kHz were used to generate the nondispersive shear-horizontal wave (SH0) in the plate. The corresponding distances $D$ in PSA became, by Eq. (2),

$$D = 6.2 \text{ mm} \quad \text{for } f = 250 \text{ kHz},$$
$$D = 4.2 \text{ mm} \quad \text{for } f = 360 \text{ kHz}$$

For all analyses the value of $c_s = 3130$ m/s was used.

The photographs taken during an experiment are shown in Fig. 8a. The zoomed photo shows assemblies of PSA-OPMTs and step motors mounted on the top of the transducers. The step motors are used to rotate the generated and measured wave directions incrementally. In fact, a LabVIEW-based program was developed to automatically rotate PSA-OPMTs by the desired amount of rotation angle. Figure 8b presents a schematic of the experimental setup. The wave signal having the Gabor pulse form [21] in Eq. (1) was generated by a function generator (Agilent33250A) and then amplified by an amplifier (RITEC RAM-5000). The output voltages of the receivers were processed by a preamplifier (Stanford Research Systems SR560) through a switching unit and sent to an oscilloscope (National Instruments 5122 high-resolution digitizers). The developed LabVIEW program was also used to automate the transmission and reception of wave signals and to perform the imaging process explained in the preceding section. A snapshot of the graphic interface of the program is shown in Fig. 8c.

### B. Imaging with Three Planar Solenoid Array-Type Orientation-Adjustable Patch-Type Magnetostrictive Transducers

Imaging by using three PSA-OPMTs will be explained first: P1 was used as the transmitter ($T_i$) and P2 and P3, as the receivers ($R_j$). Therefore, two sets of data were obtained:$I_{1,2}$ and $I_{1,3}$ from PSA-OPMT based shear-horizontal guided-wave experiments. Using $I_{1,2}$ and $I_{1,3}$ only, we will investigate the effects of the number of virtual grid points and the effects of the center frequency among others.

#### 1. *Effects of the Number of Virtual Grid Points*

Figure 9 shows the imaged results for case 1, i.e., for an plate having a single hole crack $C_1^{(1)}$. The distributions of $I_{1,2}$ and $I_{1,3}$ were calculated for different numbers of grid points, $N = 3 \times 3 = 9$, $5 \times 5 = 25$ and $17 \times 17 = 289$. The corresponding grid sizes $G$ are

$$G = 100 \text{ mm} \quad \text{for } N = 9, \quad G = 50 \text{ mm} \quad \text{for } N = 25, \quad \text{and}$$
$$G = 12.5 \text{ mm} \quad \text{for } N = 289$$

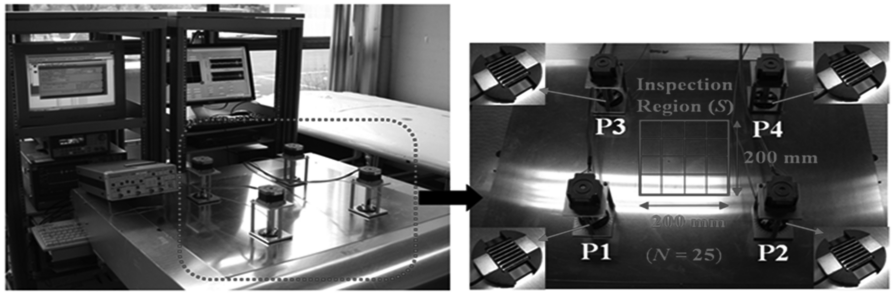


a)

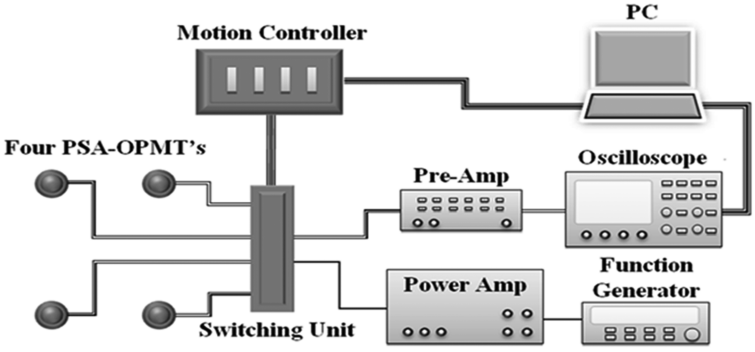


b)

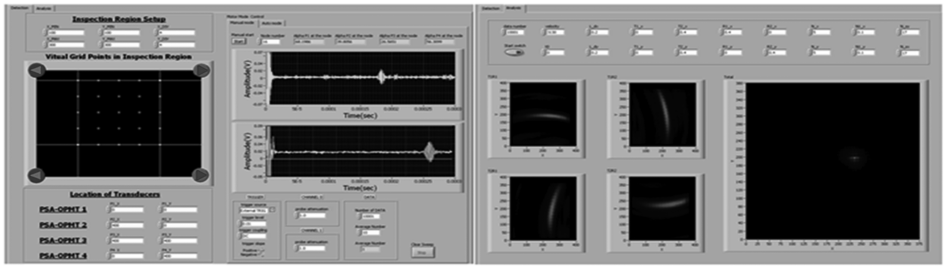


c)

**Fig. 8 a) Photographs taken during an experiment, b) schematic of the experimental setup, and c) graphical user interface front panel of the developed LabVIEW program.**

As can be seen from the processed images, small circular bright zones indicate the location of the hole $C_1^{(1)}$. The exact hole location is represented by a small circle in the figures. From Fig. 9, one can see that the proposed imaging technique successfully predicts the hole location. The image resolution improves as the number $N$ increases. The result with a small number $N = 9$ also appears to be satisfactory. Now let us consider case 2 in which a plate has two cracks $C_1^{(2)}$ and $C_2^{(2)}$. The processed images with $f = 250$ kHz by using $I = I_{1,2} \times I_{1,3}$ for different values of $N$ are shown in Fig. 10. Some improvements are achieved as $N$ increases, but a phantom crack was also found in these results. Therefore, further improvements should be made to predict crack locations accurately in case of small-sized multiple cracks.

*2. Effects of the Center Frequency*

To improve image resolution, a higher center frequency was considered. Because the beam width becomes narrower as the frequency becomes higher (see Fig. 2), the use of a higher center frequency is expected to improve image resolution. Figure 11 shows the results obtained using $f = 360$ kHz for Case 2. In comparison with the results for $f = 250$ kHz in Fig. 10, the strength of the phantom crack is reduced considerably. Especially when $N$ is large, the phantom crack has virtually disappeared. Therefore, the effects of the center frequency, equivalently, the beam width, are shown to be quite significant when a crack is small and the number of cracks is large.

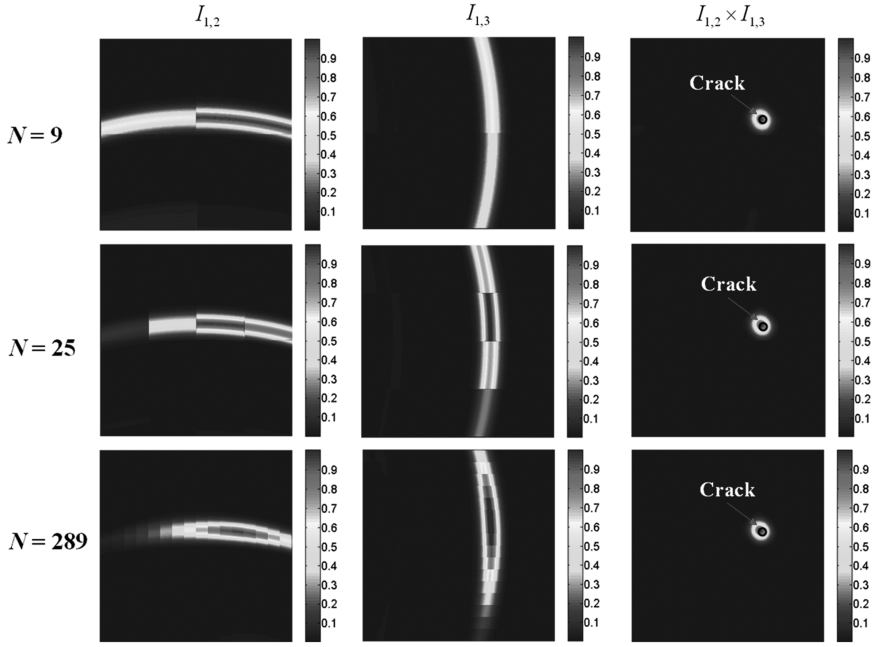


**Fig. 9 Imaging process of a 0.8 mm thick aluminum plate having a 3 mm hole $C_1^{(1)}$ by using $I_{1,2}$, $I_{1,3}$, and $I = I_{1,2} \times I_{1,3}$ for $N = 9$, 25, and 289. The center frequency of the shear-horizontal guided wave is 250 kHz.**

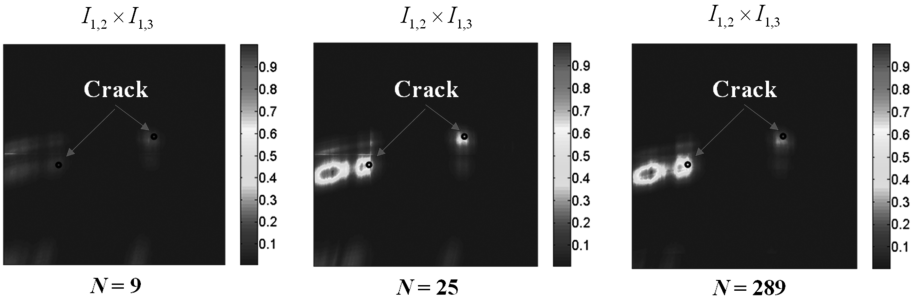


**Fig. 10 Processed images for case 2 (a plate having two cracks with a diameter of 1 mm) by using $I = I_{1,2} \times I_{1,3}$. The center frequency is 250 kHz.**

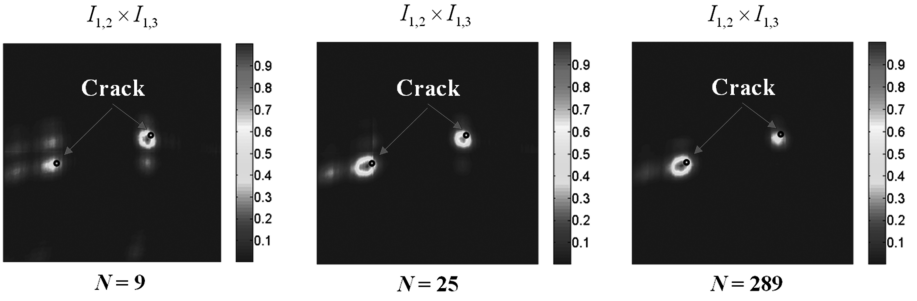


**Fig. 11 Processed images for case 2 by using the center frequency of 360 kHz.**

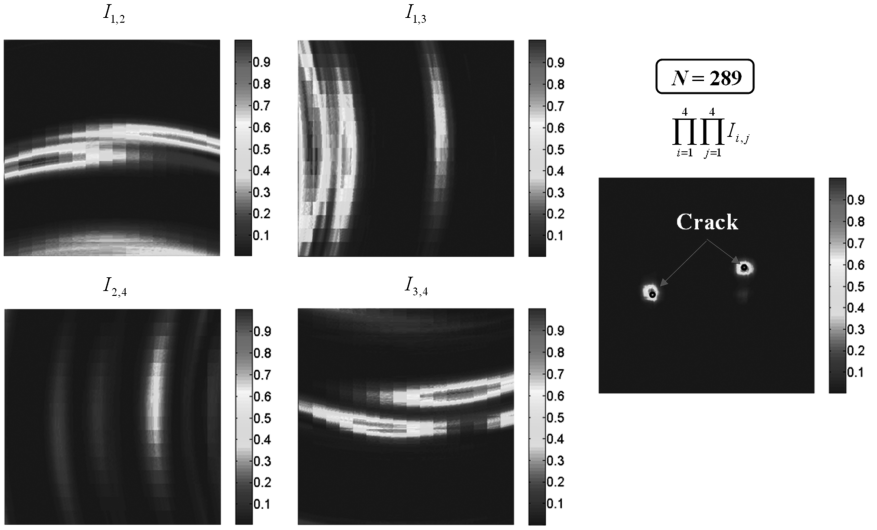


**Fig. 12 Imaging process for case 2 with $M = 4$, $N = 289$, and $f = 250$ kHz and the final image by $I = \prod_{i=1}^{4}\prod_{j=1}^{4} I_{i,j}$ $(j > i)$.**

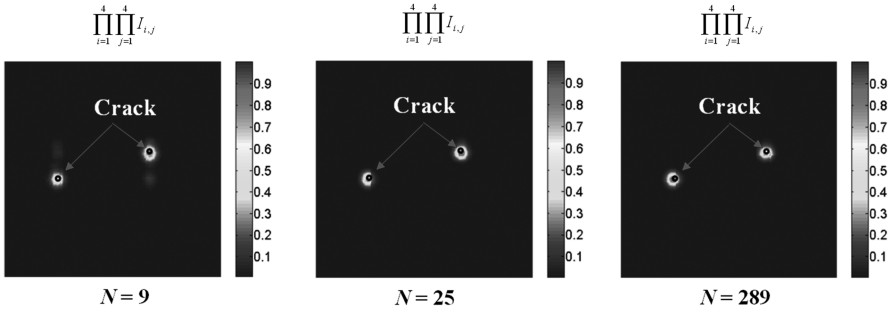


**Fig. 13 Processed images for case 2 with $M = 4$ and $f = 360$ kHz. Three different numbers $N$ of grid points are used.**

### C. Imaging with Four Planar Solenoid Array-Type Orientation-Adjustable Patch-Type Magnetostrictive Transducers

Now let us consider imaging by using four PSA-OPMTs. If four transducers are employed, the following four sets of experiments will be conducted:

$$(i, j) = (1, 2), (1, 3), (2, 4) \quad \text{and} \quad (3, 4)$$

Figure 12 shows the process of imaging for $N = 289$ and $f =$ 250 kHz. Before obtaining the image from $I = \prod_{i=1}^{4}\prod_{i=1}^{4} I_{i,j}$, (with $j > i$) $= I_{1,2} \times I_{1,3} \times I_{2,4} \times I_{3,4}$, the images by using each of $I_{1,2}$, $I_{1,3}$, $I_{2,4}$ and $I_{3,4}$ are also plotted in Fig. 12. In comparison with the processed image using $I = I_{1,2} \times I_{1,3}$ for $N = 289$ (shown in Fig. 10), the image in Fig. 12 shows substantial improvements; it is less affected by the phantom crack. However, there is still a hint of the phantom crack.

Now the imaging by using $I = I_{1,2} \times I_{1,3} \times I_{2,4} \times I_{3,4}$ for $f =$ 360 kHz is conducted and the results are plotted in Fig. 13. For $N \geq 25$, the phantom crack has virtually disappeared. Figure 13 also indicates that when a higher center frequency is used, the number of grid points appears less critical than for lower center frequencies.

Finally, we compare the prediction accuracy of hole locations for varying numbers ($M$) of the used transducers and center frequencies in case 2. For quantitative comparison, the following error measure is used

$$e = \frac{\sqrt{|(\hat{x}_c - x_c)^2 + (\hat{y}_c - y_c)^2|}}{\sqrt{2}a} \times 100 \quad (\%) \tag{16}$$

where $\sqrt{2}a$ ($a = 200$ mm) is the diagonal distance of the inspection region $S$. The symbol $e$ in Eq. (16) expresses discrepancy between the actual and estimated crack locations. In Eq. (16), $(x_c, y_c)$ and $(\hat{x}_c, \hat{y}_c)$ denote the actual and estimated crack locations, respectively. We will use $e_1$ and $e_2$ to denote the prediction errors of $C_1^{(2)}$ and $C_2^{(2)}$, respectively. Table 1 lists the numerical values of $e_i$ $(i = 1, 2)$. It shows that higher-frequency excitation and the use of more transducers help improve the prediction accuracy of crack locations. Note that it is more affected by the center frequency than the total numbers of the used transducers.

**Table 1 Discrepancy between actual and estimated crack locations for case 2 (having two cracks with diameters of 1 mm) with $N = 289$**

| | | | $C_1^{(2)}$ | $C_2^{(2)}$ | $e1$, % | $e2$, % |
|---|---|---|---|---|---|---|
| Actual crack location, mm | | | (146, 190) | (235, 215) | 0 | 0 |
| Estimated crack location $(\hat{x}_c, \hat{y}_c)$ | $\prod_{i=1}^{3}\prod_{j=1}^{3} I_{i,j}$ | 250 kHz | (117, 185) | (229, 213) | 10.45 | 2.09 |
| | | 360 kHz | (145, 188) | (232, 213) | 0.75 | 1.29 |
| | $\prod_{i=1}^{4}\prod_{j=1}^{4} I_{i,j}$ | 250 kHz | (149, 196) | (238, 215) | 2.21 | 1.10 |
| | | 360 kHz | (148, 191) | (233, 213) | 0.78 | 0.94 |

## IV. Conclusions

A pitch–catch damage detection method by using beam-focused shear-horizontal wave transducers based on the magnetostrictive principle and an imaging method using them was developed for the ultrasonic inspection of a plate structure. For focused beam directivity, specially configured transducers called the PSA-OPMTs (planar solenoid array-type orientation-adjustable patch-type magnetostrictive transducers) were employed. The findings from this study can be summarized as follows.

1. Because of the focusing characteristics of PSA-OPMT, the ultrasonic guided-wave scanning of a plate was achieved by simple automated rotation of beam focusing directions without forming a phased array. Only four transducers were used to scan a square region (200 mm $\times$ 200 mm) of a rectangular plate.

2. The used guided-wave mode was the lowest nondispersive shear wave mode. Therefore, the signal processing did not require an additional consideration of wave dispersion.

3. The scanned image resolution was most significantly affected by the center frequency. Because the higher center frequency corresponds to the shorter wavelength, the image resolution becomes higher. In the test experiment, phantom cracks observed in low-frequency imaging (250 kHz) virtually disappeared in high-frequency imaging (360 kHz). In fact, two cracks with diameters of 1 mm were clearly identified without any hint of false phantom crack images.

4. The number of virtual beam target points (or grid points) affected imaging resolution, but it was not as significant as the center frequency for the developed algorithm. The use of the largest number of grid points ($N = 289$) alone did not eliminate phantom crack images if the center frequency was low (250 kHz in the present case).

5. Obviously, the more use of transducer improved the quality of the resulting image.

The limitation of the developed method is that only the location of small circular cracks was identified. Therefore, a follow-up research on crack shape imaging needs to be conducted. Also, the inspection zone for this research was relatively small. Therefore, some advancement for covering large zones needs to be made for the practical use of the developed method. In addition, the miniaturization of the developed PSA-OPMTs should be considered for permanent transducer installation in a structure. This can be a key for online health monitoring. Currently, a study to modify the PSA-OPMT configuration for the miniaturization is ongoing.

## Acknowledgments

This research was supported by the National Creative Research Initiatives Program (Korea Science and Technology Foundation Grant No. 0420-2008-0011) contracted through the Institute of Advanced Machinery and Design at Seoul National University, Republic of Korea.

## References

[1] Zhao, X., Gao, H., Zhang, G., Ayhan, B., Yan, F., Kwan, C., and Rose, J. L., "Active Health Monitoring of an Aircraft Wing with Embedded Piezoelectric Sensor/Actuator Network: I. Defect Detection, Localization and Growth Monitoring," *Smart Materials and Structures*, Vol. 16, No. 4, 2007, pp. 1208–1217. doi: 10.1088/0964-1726/16/4/032

[2] Dalton, R. P., Cawley, P., and Lowe, M. J. S., "The Potential of Guided Waves for Monitoring Large Area of Metallic Aircraft Fuselage Structure," *Journal of Nondestructive Evaluation*, Vol. 20, No. 1, 2001, pp. 29–46. doi:10.1023/A:1010601829968

[3] Fromme, P., "Monitoring of Plate Structures Using Guided Ultrasonic Waves," *Review of Progress in Quantitative NDE*, Vol. 975, American Institute of Physics, College Park, MD, 2008, pp. 78–85.

[4] Kwun, H., and Kim, S. Y., "Magnetostrictive Sensor for Generating and Detecting Plate Guided Waves," *Journal of Pressure Vessel Technology*, Vol. 127, No. 3, 2005, pp. 284–289. doi:10.1115/1.1991874

[5] Lee, B. C., and Staszewski, W. J., "Lamb Wave Propagation Modeling for Damage Detection: II. Damage Monitoring Strategy," *Smart Materials and Structures*, Vol. 16, No. 2, 2007, pp. 260–274. doi: 10.1088/0964-1726/16/2/004

[6] Giurgiutiu, V., Yu, L., Kendall, J. R., and Jenkins, C., "In Situ Imaging of Crack Growth with Piezoelectric-Wafer Active Sensors," *AIAA Journal*, Vol. 45, No. 11, 2007, pp. 2758–2769. doi:10.2514/1.30798

[7] Salas, K. I., and Cesnik, C. E. S., "Guided Wave Experimentation using CLoVER Transducers for Structural Health Monitoring," AIAA Paper 2008-1970, 2008.

[8] Fromme, P., Wilcox, P. D., Lowe, M. J. S., and Cawley, P., "On the Development and Testing of a Guided Ultrasonic Wave Array for Structural Health Monitoring," *IEEE Transactions on Ultrasonics, Ferroelectrics, and Frequency Control*, Vol. 53, No. 4, 2006, pp. 777–785.

[9] Purekar, A. S., Pines, D. J., Sundararaman, S., and Adams, D. E., "Directional Piezoelectric Phased Array Filters for Detecting Damage in Isotropic Plates," *Smart Materials and Structures*, Vol. 13, No. 4, 2004, pp. 838–850. doi: 10.1088/0964-1726/13/4/022

[10] Giurgiutiu, V., and Yu, L., "In Situ 2-D Piezoelectric Wafer Active Sensors Arrays for Guided Wave Damage Detection," *Ultrasonics*, Vol. 48, No. 2, 2008, pp. 117–134.

[11] Rajagopalan, J., Balasubramaniam, K., and Krishnamurthy, C. V., "A Single Transmitter Multi-Receiver (STMR) PZT Array for Guided Ultrasonic Wave Based Structural Health Monitoring of Large Isotropic Plate Structures," *Smart Materials and Structures*, Vol. 15, No. 5, 2006, pp. 1190–1196. doi: 10.1088/0964-1726/15/5/005

[12] Wilcox, P. D., Lowe, M., and Cawley, P., "Omnidirectional Guided Wave Inspection of Large Metallic Plate Structures Using an EMAT Array," *IEEE Transactions on Ultrasonics, Ferroelectrics, and Frequency Control*, Vol. 52, No. 4,2005, pp. 653–665. doi:10.1109/TUFFC.2005.1428048

[13] Lee, J. S., Cho, S. H., and Kim, Y. Y., "Beam-Focused Shear-Horizontal Wave Generation in a Plate by a Circular Magnetostrictive Patch Transducer Employing a Planar Solenoid Array," *Smart Materials and Structures*, Vol. 18, No. 1, 2009. doi: 10.1088/0964-1726/18/1/015009

[14] Giurgiutiu, V., "Tuned Lamb Wave Excitation and Detection with Piezoelectric Wafer Active Sensors for Structural Health Monitoring," *Journal of Intelligent Material Systems and Structures*, Vol. 16, No. 4, 2005, pp. 291–305. doi:10.1177/1045389X05050106

[15] Xu, B., and Giurgiutiu, V., "Single Mode Tuning Effects on Lamb Wave Time Reversal with Piezoelectric Wafer Active Sensors for Structural Health Monitoring," *Journal of Nondestructive Evaluation*, Vol. 26, No. 2-4, 2007, pp. 123–134. doi:10.1007/s10921-007-0027-8

[16] Rajagopalan, J., Balasubramaniam, K., and Krishnamurthy, C. V., "A Phase Reconstruction Algorithm for Lamb Wave Based Structural Health Monitoring of Anisotropic Multilayered Composite Plates," *Journal of the Acoustical Society of America*, Vol. 119, No. 2, 2006, pp. 872–878. doi:10.1121/1.2149775

[17] Sicard, R., Goyette, J., and Zellouf, D., "A SAFT Algorithm for Lamb Wave Imaging of Isotropic Plate-Like Structures," *Ultrasonics*, Vol. 39, No. 7, 2002, pp. 487–494. doi:10.1016/S0041-624X(01)00087-7

[18] Bozorth, R. M., *Ferromagnetism*, IEEE press, New York, 1993, pp. 627–655.

[19] Tzannes, N. S., "Joule and Wiedemann Effects–The Simultaneous Generation of Longitudinal and Torsional Stress Pulses in Magnetostrictive Materials," *IEEE Transactions on Sonics and Ultrasonics*, Vol. 13, No. 2, 1966, pp. 33–41.

[20] Thompson, R. B., "Generation of Horizontally Polarized Shear Waves in Ferromagnetic Materials Using Magnetostrictively Coupled Meander-Coil Electromagnetic Transducers," *Applied Physics Letters*, Vol. 34, No. 2, 1979, pp. 175–177. doi:10.1063/1.90719

[21] Gabor, D., "Theory of Communication," *J. IEE*, Vol. 93, No. 26, 1946, pp. 429–457.

[22] Yu, L., and Giurgiutiu, V., "In-Situ Optimized PWAS Phased Arrays for Lamb Wave Structural Health Monitoring," *Journal of Mechanics of Materials and Structures*, Vol. 2, No. 3, 2007, pp. 459–488. doi:10.2140/jomms.2007.2.459

C. Cesnik
*Associate Editor*